

Baryon distribution in relativistic heavy-ion collisions

Cheuk-Yin Wong

Oak Ridge National Laboratory, Oak Ridge, Tennessee 37830

(Received 9 February 1984)

In order to determine whether a pure quark-gluon plasma with no net baryon density can be formed in the central rapidity region in relativistic heavy-ion collisions, we estimate the baryon distribution by using a Glauber-type multiple-collision model in which the nucleons of one nucleus degrade in energy as they make collisions with nucleons in the other nucleus. As a test of this model, we study first nucleon-nucleus collisions at 100 GeV/ c and compare the theoretical results with the experimental data of Barton *et al.* The results are then generalized to study the baryon distribution in nucleus-nucleus collisions. It is found that in the head-on collision of two heavy nuclei ($A \geq 100$), the baryon rapidity distributions have broad peaks and extend well into the central rapidity region. The energy density of the baryon in the central rapidity region is about 5–6% of the total energy density at a center-of-mass energy of 30 GeV per nucleon and decreases to about 2–3% at a center-of-mass energy of 100 GeV per nucleon. The stopping power for a baryon in nuclear matter is extracted.

I. INTRODUCTION

Recently, there has been much interest in relativistic heavy-ion collisions at an energy of many tens of GeV per nucleon in the c.m. system^{1–6} It was suggested that in energetic reactions involving large nuclei, a large number of baryon-baryon collisions take place in a small region of space and at about the same time (in the center-of-mass frame). With each baryon-baryon collision producing a large number of hadronic particles, the total energy density in the central rapidity region is high and may exceed the critical energy density for a phase transition between ordinary confined matter and the unconfined quark-gluon plasma.⁷ Experimental searches and investigations of the quark-gluon plasma will provide a new insight in quark confinement and the evolution of the early universe.⁸

Previously, the initial energy density in the central rapidity region was estimated using different models.^{1,4,6} A phenomenological Glauber-type multiple-collision model⁶ gives quantitatively reasonable agreement for the multiplicity in the central rapidity region. The energy density inferred therefrom is high. For example, for the head-on collision of ²³⁸U on ²³⁸U at 30 GeV per nucleon in the center-of-mass system, the maximum energy density is about 10 GeV/fm³. The initial energy density goes as $A^{1/3}B^{1/3}$ for the collision of two nuclei with mass numbers A and B , and is rather insensitive to impact parameters.

As the fraction of baryons in the early universe was small,⁸ it seems desirable to design a heavy-ion collider such that at the available bombarding energies when the energy density in the central rapidity is high enough for a quark-gluon-plasma phase transition, there is no net baryon density there. Whether this is possible depends on the baryon distribution. Recent investigations from nucleon-nucleus data reveal that the average downward shift of the projectile-baryon rapidity is quite large.⁹ In Ref. 9, however, the widths of the distribution were not

estimated. The choice on the optimal bombarding energy depends not only on the average rapidity loss but also on the width of the momentum distribution of the baryons. A small width would allow the two fragmentation regions to separate from each other when the bombarding energy is high enough, thereby allowing the formation of a pure quark-gluon plasma. On the other hand, a large width will make it impossible to have a pure quark-gluon plasma without some baryon impurities.

Not much is known about the baryon momentum distribution in highly relativistic heavy-ion reactions. A previous analysis¹⁰ made use of only mean loss per collision and imposed the constraint that in the laboratory frame a projectile nucleon could not be slowed down below the speed of the center-of-mass frame. The latter constraint does not arise from energy-conservation conditions and may not be realistic. The use of only average loss per collision without folding the width of the distribution is not a good description because of the large width in the momentum distribution in nucleon-nucleon collisions.

We shall study the baryon distribution¹¹ using a Glauber-type multiple-collision model^{12,13} in which a nucleon in one nucleus makes many inelastic collisions with nucleons in the other nucleus, the probability of a collision being given by the thickness function and the nucleon-nucleon inelastic cross section. The nucleon may change its identity during its passage through the nucleus, but its baryon number remains unchanged. The relation between the Glauber multiple-collision expansion and the high-order Feynman diagrams in a hadron-nucleus collision was first demonstrated by Gribov and studied further by other authors.^{14–17} The multiple-collision model is a reasonable description if the range of nucleon-nucleon interaction is short compared with the spacing between nucleons. In the laboratory frame, the latter quantity is of the order of 2 fm, while the range of nucleon-nucleon interaction is about 0.7 fm and decreases with increasing energy. It appears that a multiple-collision model may be a

reasonable concept. Indeed, the use of the Glauber model gives the correct nucleon-nucleus absorption cross section and its A dependence.^{18,19} A Glauber model, with the additional assumption of no secondary collision of the produced particles but no adjustable parameters, gives a total multiplicity consistently within 30%.^{6,20,21} A multiple-collision picture of the Glauber type appears to have approximate validity in describing the gross features of the reaction process. However, there are complications when we try to use the model to examine the finer details of high-energy nucleus-nucleus collisions. In these collisions, most of the particles are produced outside the nuclei,²² while energies of the baryons are apparently degraded inside the nucleus. How are the energies of baryons degraded as they pass through the other nucleus, and how does the degradation affect the production process? How does one account for 30% difference in total multiplicity and change of shape of the rapidity density?^{6,20,21} Different assumptions will lead to different model results. In the multichain model^{23–25} the momentum distribution of the colliding baryons comes from a coherent but unknown partition of the energy among the collision chains. In Ref. 24, it is given by a postulated probability function $P(\lambda) = \alpha \lambda^{\alpha-1}$, where α is a free parameter and found to be ~ 6 . In some other work on the multichain model,²⁵ the momentum distribution is parametrized in terms of an equal partition of the beam momentum among the arms of the chain. However, there are many approximations in the numerical calculations which make their conclusions uncertain. Some recent theoretical work^{26,27} studied $pA \rightarrow pX$ data in terms of a basic degradation function involving an adjustable parameter and postulated a relation of $A^{2/3}$ between the invariant pA cross section and the mass number A .

As the production of most of the particles occurs outside the nucleus while collisions occur inside the nucleus, it appears that by causality the production of particles from one collision is affected by the latter collisions. However, as we observe in the laboratory frame, the large mean separation between nucleons in nuclear matter and the small range of nucleon-nucleon interaction makes it plausible that for a given collision, much of the influence on energy degradation and the particle production processes from later collisions along the chain is small. To a first approximation, then, this small influence can be neglected. One has then a multiple-collision model in which each baryon-baryon collision produces particles and degrades energies as if the collision occurs in free space. In this phenomenological model, all the baryon-baryon collisions are independent, and their effects are incoherently superimposed. If the baryon-baryon data are known, there will be no free parameters; all the information must come from the relevant nucleon-nucleon (or baryon-baryon) experimental data. This model does not include coherent effects such as arising from the interference due to later collisions, the mean-field hydrodynamical-type compression,²⁸ the formation zone of Landau and Pomeranchuk,²⁹ inside-outside cascade,³⁰ the formation of the quark-gluon plasma, etc. This multiple-collision model with no free parameters can serve as a reference model (a benchmark, so to speak) whereby

any coherent or other effect, if it exists at all, may manifest itself as systematic deviations of the experimental data from model predictions. It is important to test this reference model in cases where there are experimental data available, not only to judge the degree of approximate validity of the model, but also to see if there is any need for the introduction of additional corrections or modifications due to coherent or other effects. In this paper we shall focus our attention on the longitudinal-momentum distribution in terms of the Feynman scaling variable x . The transverse-momentum distribution is approximately an exponential or a Gaussian with a mean transverse momentum of about 0.3–0.4 GeV/ c (Refs. 31 and 32).

In our studies of the nucleus-nucleus collisions, we are very much aided by a remarkable feature of the nucleon-nucleon inelastic differential cross section.^{31,9} In terms of the Feynman scaling variable x , the inelastic cross section $d\sigma/dx$ is approximately a constant. This is to say, a nucleon after an inelastic collision can be found within the whole range of fractional momentum with about equal probability. In terms of x , the width of the momentum distribution after a nucleon-nucleon collision is very wide indeed. This simple feature simplifies the theoretical analysis. Furthermore, the differential cross sections are known to obey Feynman scaling.³³ That is, the approximate constancy of $d\sigma/dx$ is independent of the nucleon-nucleon bombarding energy if the energy is sufficiently high. Thus, in the discussion of nucleon-nucleus collision, because of Feynman scaling, we do not need to follow the energy of relative motion of each baryon-nucleon collision; it suffices to follow the x distribution by folding the x distributions of all previous baryon-nucleon collisions. With some simplifying assumptions, it also allows us to treat the projectile nucleons separately from the target nucleons in nucleus-nucleus collisions.

As a point of calibration of our model, we study first the differential cross section in nucleon-nucleus collisions and compare the theoretical results with the experimental data of Barton *et al.*³² The results are then generalized to study the baryon distribution in nucleus-nucleus collisions.

This paper is organized as follows. In Sec. II we review the experimental data on nucleon-nucleon collisions and examine the remarkable feature of an approximately constant $d\sigma/dx$ as a function of x . We shall assume that $d\sigma/dx$ is a constant and obtain the momentum distributions in x and in rapidity y for nucleons after n nucleon-nucleon (or baryon-baryon) inelastic collisions. They are given in analytic forms in Sec. III. We study in Sec. IV the implication of these momentum distributions on the stopping-power law of baryons traversing nuclear matter. In Sec. V we show how the momentum distributions are modified due to energy-momentum-conservation constraints. These results, combined with the probability for having collisions of different frequencies, allow one to calculate the inelastic differential cross section in nucleon-nucleus collisions. We compare the theoretical results with the experimental data in Sec. VI and find good agreement. Treating a nucleus-nucleus collision as the collision of an ensemble of spatially correlated nucleons

with a nucleus, we obtain in Sec. VII the rapidity distribution of baryons in a head-on nucleus-nucleus collision of equal-mass nuclei. We discuss the effect of Fermi motion on the distribution in Sec. VIII. In Sec. IX we relate the resultant rapidity distribution to the spatial density of baryons at the proper time of 1 fm/c when the produced particles begin to emerge. Numerical results are given in Sec. X for two different bombarding energies. In Sec. XI we discuss the implication of the present results on the question of energy requirements for relativistic heavy-ion colliders.

II. MOMENTUM DISTRIBUTION IN NUCLEON-NUCLEON COLLISIONS

In either the nucleon-nucleus collision or the nucleus-nucleus collision, the basic process is the nucleon-nucleon collision. Experimental information on nucleon-nucleon collisions reveals much about the degradation of the energy of a baryon when it collides with another baryon. It forms the basis for all subsequent discussions.

In a nucleon-nucleon collision, the incident nucleon can be scattered elastically or inelastically. At high energies, the inelastic scattering, with the production of a large number of particles, is the predominant mechanism for slowing down the incident nucleon. The elastic scattering has a negligible effect in energy degradation. This can be demonstrated quantitatively in the following way. We consider the collision of $a+b \rightarrow c+d$ with b the incident (beam) nucleon and c the detected particle. We use the notation that the momentum has the same label as the particle. That is, the energy-momentum four-vector of b is $(\vec{b}_0, \vec{b}_T, b_Z)$ and the energy-momentum four-vector of c is (c_0, \vec{c}_T, c_Z) . In the infinite-momentum-frame representation, the energy-momentum four-vectors b and c can be rewritten as

$$b = \left[p_1 + \frac{b^2}{4p_1}, \vec{0}, p_1 - \frac{b^2}{4p_1} \right], \quad (2.1)$$

and

$$c = \left[xp_1 + \frac{c^2 + \vec{c}_T^2}{4xp_1}, \vec{c}_T, xp_1 - \frac{c^2 + \vec{c}_T^2}{4p_1} \right], \quad (2.2)$$

where x , the Feynman scaling variable,

$$x = \frac{c_0 + c_z}{b_0 + b_z}, \quad (2.3)$$

is the (longitudinal) momentum fraction of the detected particle c with respect to the (parent) beam particle b and $b^2 = b_0^2 - \vec{b}^2$. The momentum fraction x is independent of the coordinate frames. The momentum parameter p_1 , however, depends on the choice of the coordinate system. In the center-of-mass frame, p_1 is given by

$$p_1 = [s + b^2 - a^2 + \lambda(s, a^2, b^2)] / 4\sqrt{s}, \quad (2.4)$$

where the covariant quantity s is

$$s = (a + b)^2 \quad (2.5)$$

and

$$\lambda(s, a^2, b^2) = s^2 + a^4 + b^4 - 2(sa^2 + sb^2 + a^2b^2). \quad (2.6)$$

For the elastic nucleon-nucleon scattering, the invariant quantity $t = (b - c)^2$ is related to x by

$$x = 1 - \frac{t}{b^2 - 4p_1^2}. \quad (2.7)$$

The elastic cross section has the form³⁴

$$\frac{d\sigma}{dt} = Ae^{Bt}. \quad (2.8)$$

The average \bar{x} after an elastic scattering is therefore

$$\bar{x} = \int xe^{Bt} dt / \int e^{Bt} dt = 1 + \frac{1}{B(b^2 - 4p_1^2)}. \quad (2.9)$$

At an incident laboratory momentum of 100 GeV/c the slope parameter³⁴ is $B \sim 12$ (GeV/c)⁻² and we have

$$1 - \bar{x} = 0.00053. \quad (2.10)$$

Thus, the average fractional loss of momentum due to elastic scattering is small indeed.

The fractional loss of momentum due to an inelastic scattering is, however, very substantial. In an inelastic scattering, a large number of particles are produced with a plateau in the central rapidity region which extends to $y \sim \pm 3$ in the center-of-mass frame^{35,36} (for collisions with $\sqrt{s} \sim 50$ GeV). These particles carry away a substantial amount of energy and momentum, and the energy momentum of the incident baryon is much degraded. The degree of degradation is measured by the $pp \rightarrow pX$ cross section as a function of x and p_T . The p_T dependence varies slightly with the value of x . In the present study, we shall focus our attention on the x dependence of the momentum distribution by considering the differential cross section integrated over the transverse momenta p_T . The cross section³¹ $d\sigma/dx$ for inelastic collision at $p_{\text{lab}} = 100$ and 175 GeV/c is shown in Fig. 1. As one observes, except for a small region around $x \sim 1.0$, the cross

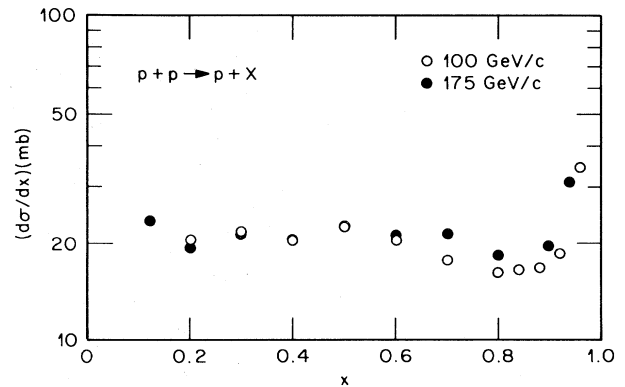


FIG. 1. Cross section $d\sigma/dx$ for the reaction $pp \rightarrow pX$ after integration over the transverse momenta p_T . Data are from Ref. 31. Note the approximate constancy of the cross section.

section is quite flat. There are small kinematically forbidden regions very close to $x=1.0$ and 0 (which we shall neglect for the moment but shall go into some detail later). There is also a small contribution of protons near the region $x=0$ from proton-antiproton pair production which we do not need to consider. The result of Fig. 1 suggests that it is reasonable to make the approximation⁹ of a constant $pp \rightarrow px$ differential cross section that is independent of x :

$$\frac{d\sigma}{dx} \sim 20 \text{ mb}. \quad (2.11)$$

The differential cross section $d\sigma/dx$ for finding other baryons is expected to have the same feature; that is, $d\sigma/dx$ is approximately independent of x . The probability distribution $w(x)$ for finding a "leading-particle" baryon with momentum fraction x after an inelastic nucleon-nucleon or a baryon-baryon collision can be approximated by

$$w(x) = \frac{d\sigma}{dx} / \int_0^1 \frac{d\sigma}{dx} dx = 1. \quad (2.12)$$

This means that in an inelastic collision between a baryon and another baryon, the fractional momentum of the resultant baryon x ranges through all possible values which occur with equal probability. On the average, the momentum fraction x after one inelastic collision is one-half of its original value. The loss of momentum after an inelastic collision is so much larger than the loss of momentum after an elastic collision that we can safely neglect the elastic collision in our consideration of the baryon momentum distribution. Henceforth, the terms nucleon-nucleon collision and baryon-baryon collision shall mean nucleon-nucleon *inelastic* collision or baryon-baryon *inelastic* collision, respectively.

As is well known, when energy is sufficiently high, the cross sections obey Feynman scaling such that when expressed as a function of x , the invariant cross section is approximately independent of energy (or at least only very mildly dependent).³³ This remarkable feature, together with the constancy of the differential cross section $d\sigma/dx$, makes it simple to obtain the spectra of baryons in p - A or A - A collisions.

III. MOMENTUM DISTRIBUTION AFTER MANY NUCLEON-NUCLEON INELASTIC COLLISIONS

In this section we shall assume first Feynman scaling and no kinematic constraints on the value of x . The momentum distribution of the incident nucleon after n inelastic collisions $D^{(n)}(x_n)$ is related to that after $(n-1)$ inelastic collisions $D^{(n-1)}(x_{n-1})$ by

$$D^{(n)}(x_n) = \int dx_{n-1} D^{(n-1)}(x_{n-1}) w(x_{n-1}, x_n), \quad (3.1)$$

where the function $w(x_{n-1}, x_n)$ is the probability for finding a "leading" baryon with a final Feynman scaling variable x_n after a nucleon-nucleon or a baryon-baryon inelastic collision if the initial scaling variable is x_{n-1} . From experimental data of nucleon-nucleon collision (2.12), the normalized probability distribution $w(x_{n-1}, x_n)$ can be approximated by

$$w(x_{n-1}, x_n) = \theta(x_{n-1} - x_n) \theta(x_n) / x_{n-1}. \quad (3.2)$$

The functions w and $D^{(n)}$ are normalized according to

$$\int w(x_{n-1}, x_n) dx_n = \int D^{(n)}(x_n) dx_n = 1. \quad (3.3)$$

Initially, the source momentum distribution is a δ function

$$D^{(0)}(x) = \delta(x-1) \quad (3.4)$$

and the momentum distribution after n collisions $D^{(n)}(x)$ can be integrated out to give

$$D^{(1)}(x) = \theta(1-x) \theta(x) \quad (3.5)$$

and

$$D^{(n)}(x) = \frac{[-\ln(x)]^{n-1}}{(n-1)!} \theta(1-x) \theta(x). \quad (3.6)$$

The distribution function shows that as the number of collisions increases, the probability of having a small value of x increases by a power of $[-\ln(x)]$. Although $D^{(n)}(x)$ becomes very large near $x=0$, the integral (3.3) nevertheless converges. For a given value of x , the distribution is a Poisson distribution in n with $\langle n-1 \rangle = -\ln(x)$. It is interesting to note that this distribution is similar in form to the distribution of neutron energies in the slowing down of neutrons in a reactor.³⁷

The distribution function (3.6) produces the following average value of x after n collisions:

$$\bar{x}_n = \left(\frac{1}{2}\right)^n. \quad (3.7)$$

Therefore, on the average, the x value of a baryon decreases by a factor of $\frac{1}{2}$ every time the baryon makes an inelastic collision.

Besides the Feynman scaling variable x , there is a complementary rapidity variable y defined by

$$y = \frac{1}{2} \ln \frac{c_0 + c_z}{c_0 - c_z}, \quad (3.8)$$

where c is the detected particle (proton in this case). Therefore x and y are related by

$$\ln x = y - y_i + \ln(m_T/m), \quad (3.9)$$

where

$$m_T = (m^2 + c_T^2)^{1/2}, \quad (3.10)$$

m is the mass of detected particle c , and y_i is the rapidity of the incident particle. As c_T is of the order of 0.400 GeV/ c and $\ln(m_T/m) = 0.083$, it is reasonable to neglect henceforth the term of $\ln(m_T/m)$ of Eq. (3.9) in high-energy collisions where the range of y is of the order of 10–20. The Feynman scaling variable x gives an expanded representation of the region near $x=1$, but is rather compressed near the region $x=0$. On the other hand, the rapidity variable y gives an expanded representation of the region around $x=0$, but is rather compressed near the region $x \simeq 1$. It is necessary to use both variables to provide a good representation for the entire region.

From the distribution function $D^{(n)}(x)$, we obtain the

distribution functions as a function of the rapidity variable y as

$$D^{(0)}(y) = \delta(y - y_B) \quad (3.11)$$

and

$$D^{(n)}(y) = \frac{e^{y-y_B}(y_B-y)^{n-1}}{(n-1)!} \theta(y_B-y) \quad \text{for } n \geq 1, \quad (3.12)$$

where y_B is the beam rapidity. The distribution function is normalized according to

$$\int D^{(n)}(y) dy = 1. \quad (3.13)$$

For $n \geq 2$ the rapidity distribution has a peak located at

$$y_{\text{peak}} - y_B = -(n-1) \quad (3.14)$$

and a full width at half maximum of $\sqrt{n-1}$. The average value of y after n inelastic collisions is

$$\bar{y}_n = y_B - n. \quad (3.15)$$

Therefore, on the average, the rapidity variable of a baryon decreases by unity every time the baryon makes an inelastic collision [cf. Eq. (9.8) of Ref. 37]. The width of the distribution increases as $\sqrt{n-1}$. The greater the number of nucleon-nucleon collisions, the greater are the shift and the width of the distribution. One expects therefore that as the nuclear mass increases, the shift and the width of the distribution also increase.

IV. NUCLEAR STOPPING POWER

Equations (3.7) and (3.15) relate the average values of \bar{x}_n and \bar{y}_n to the number of baryon-baryon collisions. The quantity \bar{x}_n is frame independent. Although \bar{y}_n depends on the frame of reference, the difference $\bar{y}_n - y_B$ for Eq. (3.15) is independent of the frame of reference. These two equations can be considered the relativistic stopping-power equations for a baryon traveling in nuclear matter. In differential forms, these stopping-power equations are

$$\frac{d\bar{x}_n}{dn} = -(\ln 2)\bar{x}_n \quad (4.1)$$

and

$$\frac{d\bar{y}_n}{dn} = -1. \quad (4.2)$$

The stopping-power equation for \bar{x}_n is not as useful as the stopping-power equation for \bar{y}_n because of the large width for the x distribution. For example, after one collision, the x values are distributed uniformly over the entire range of x ; in contrast, the corresponding width in y is still quite narrow in y compared to the whole range of y . We shall restrict our discussion to the stopping-power equation for \bar{y}_n .

We can compare the differential form of the stopping-power law (4.2) with that for the bremsstrahlung of electrons. For that purpose, it is convenient to work in the frame in which the nuclear matter is at rest. By definition, the energy of the baryon at the rapidity \bar{y}_n is

$$E = m_T \cosh \bar{y}_n, \quad (4.3)$$

and the stopping-power equation (4.2) becomes

$$\frac{dE}{dn} = - \left[1 - \left[\frac{m_T}{E} \right]^2 \right]^{1/2} E. \quad (4.4)$$

In terms of the longitudinal coordinate z , the stopping-power equation is

$$\frac{dE}{dz} = -\rho_0 \sigma_{\text{in}} \left[1 - \left[\frac{m_T}{E} \right]^2 \right]^{1/2} E, \quad (4.5)$$

where ρ_0 is the (proper) nuclear-matter number density (~ 0.14 nucleons/fm³). The degradation length λ is therefore

$$\lambda = - \frac{dE}{E dz} = \rho_0 \sigma_{\text{in}} \left[1 - \left[\frac{m_T}{E} \right]^2 \right]^{1/2}. \quad (4.6)$$

At high energies in the laboratory system, the term in the square brackets is very nearly unity. The energy loss of the baryon per unit length is proportional to the energy of the baryon and the degradation length is 2.3 fm. This degradation length is much shorter than the value of 17 fm obtained with very different concepts and approximations.²⁶

The stopping-power equation for an electron in a medium is given by^{38,39}

$$\frac{dE(z)}{dz} = -\rho_0 \sigma_{\text{rad}} E, \quad (4.7)$$

where σ_{rad} , the total radiation cross section, becomes nearly energy independent as the electron energy becomes much greater than the rest mass. A comparison of (4.5) and (4.7) shows the similarity which strongly suggests that the particle-producing mechanism and energy degradation in nucleon-nucleon collision is a bremsstrahlung-type process. The incident nucleon interacts with the radiation field of QCD and also with the other nucleon. The latter interaction alters the speed of the incident nucleon. Subsequent deceleration leads to radiation which materializes into mesons.

Although the equations of stopping power are similar, there is a difference in the bremsstrahlung of electrons and the nucleon-nucleon collision. In electron bremsstrahlung, the production of one energetic photon in an electron-atom collision is most probable and the production of two or more energetic photons is a rather rare event. The ratio of the cross section for the production of n energetic photons to a single energetic photon goes as $(e^2/\hbar c)^n$. In contrast, in a nucleon-nucleon collision, the average multiplicity of produced energetic particles is about 10 for a center-of-mass energy of $\sqrt{s} \sim 30$ GeV. This difference is due to the small coupling constant in QED and a much larger coupling constant in QCD.

V. MOMENTUM DISTRIBUTION WITH KINEMATIC CONSTRAINTS

The discussions in the preceding sections assume that x (and y) can assume all possible values in the closed interval $[0,1]$ (and $[-\infty, y_B]$) without constraint. In reality,

the values of x or y are constrained by the requirement of energy and momentum conservation. The case of no kinematic constraint is of interest only in the extremely-high-energy limit where the region under consideration is far from the region affected by the constraint.

In the collision process of $a+b \rightarrow c+X$ with $m_a=m_b=m_c=m$, it can be shown that the energy-conservation condition becomes a quadratic equation in x . The range of x values allowed by the energy-conservation condition is $x_L \leq x \leq x_U$ where x_L and x_U are given by

$$\begin{pmatrix} x_L \\ x_U \end{pmatrix} = \frac{1}{2} \left[\alpha \mp \left(\alpha^2 - \frac{m_{cT}^2}{p_1^2} \right)^{1/2} \right]. \quad (5.1)$$

In the above equation, the negative sign is for the lower limit x_L and the positive sign for the upper limit x_U . The quantity α is

$$\alpha = \left[1 + \frac{m^2}{4p_1^2} \right] \left[1 + \frac{m^2 - X_{\min}^2}{4p_1^2} \left[1 + \frac{m^2}{4p_1^2} \right]^{-2} \right] \quad (5.2)$$

with p_1 given by Eq. (2.4) and X_{\min}^2 the minimum value of X^2 for the unobserved particle(s) X . In the case of $p_1^2 \gg (m^2 \text{ or } X_{\min}^2)$ which we shall assume, we have

$$x_L \cong \frac{m_{cT}^2}{4p_1^2} \cong \frac{m}{(b_0 + b_z)_{\text{lab}}} \left[\frac{m_{cT}}{m} \right]^2 \quad (5.3)$$

and

$$x_U \cong 1 - \frac{X_{\min}^2 - 2m^2 + m_{cT}^2}{4p_1^2}. \quad (5.4)$$

The lower bound of x , as given by Eq. (5.3), corresponds approximately to a nucleon completely stopped in the laboratory frame. That is, in the laboratory frame the detected baryon c has zero momentum and has approximately the target rapidity y_T .

Although there are two limits on x , the effects of the constraint due to the two limits are quite different. The difference between x_U and unity is approximately $m_p m / 2p_1^2$ which is much smaller than unity for collisions in the region of many tens of GeV per nucleon (in the c.m. system). The corresponding difference in rapidity is a very small fraction of a unit of rapidity. The situation is very different for the other limit. Although the lower limit x_L is a small fraction of unity, the difference between x_L and 0 corresponds to an infinite difference in the rapidity variable y . For these reasons, we shall not distinguish the upper limit x_U and unity but shall keep the lower limit x_L as given by Eq. (5.3) so that x is confined by $x_L \leq x \leq 1$. The corresponding rapidity variable y is then limited by $y_T \leq y \leq y_i$, where y_i is the rapidity of the incident baryon.

The experimental differential cross section $d\sigma/dx$ as a function of x is approximately a constant. Therefore, the probability $w(x_{n-1}, x_n)$ for finding a leading baryon with a final Feynman scaling variable x_n , after a nucleon-nucleon or baryon-baryon inelastic collision if the initial scaling variable is x_{n-1} , is

$$w(x_{n-1}, x_n) = \theta(x_{n-1} - x_n) \theta(x_n - x_L) / (x_{n-1} - x_L). \quad (5.5)$$

The corresponding probability distribution in y_i after a baryon-baryon collision for a baryon with initial rapidity y_{i-1} incident on a target with target rapidity y_T is

$$w(y_{i-1}, y_i) = \frac{\exp(y_i - y_{i-1})}{1 - \exp(y_T - y_{i-1})} \theta(y_i - y_T) \theta(y_{i-1} - y_i). \quad (5.6)$$

From Eq. (3.1), for the case of a single incident proton with an initial sharp momentum distribution $\delta(x-1)$, the momentum distribution of the baryon after n inelastic collisions is

$$D^{(n)}(x) = \frac{1}{1-x_L} \frac{1}{(n-1)!} \left[-\ln \left[\frac{x-x_L}{1-x_L} \right] \right]^{(n-1)} \times \theta(1-x) \theta(x-x_L). \quad (5.7)$$

The corresponding distribution for y is

$$D^{(n)}(y) = \frac{e^{y-y_B}}{1-e^{y_T-y_B}} \frac{1}{(n-1)!} \left[-\ln \left[\frac{e^y - e^{y_T}}{e^{y_B} - e^{y_T}} \right] \right]^{(n-1)} \times \theta(y_B - y) \theta(y - y_T). \quad (5.8)$$

All the distribution functions are normalized according to

$$\begin{aligned} \int w(x_{n-1}, x_n) dx_n &= \int w(y_{n-1}, y_n) dy_n \\ &= \int D^{(n)}(x) dx = \int D^{(n)}(y) dy = 1. \end{aligned}$$

It is easy to see that in the infinite-energy limit the results of Eqs. (5.7) and (5.8) reduce to the previous results of Eqs. (3.6) and (3.12).

VI. MOMENTUM DISTRIBUTION IN NUCLEON-NUCLEUS COLLISIONS

In the reaction $pA \rightarrow bX$ where A is the target nucleus with mass number A and b is a baryon, the inelastic cross section $d\sigma^{pA}/dx$ can be obtained by probability arguments. We introduce the thickness function¹² for the collision of a beam nucleus B with a target nucleus A as

$$T(\vec{b}) = \int \rho_A(\vec{b}_A, z) \rho_B(\vec{b}_B, z_B) t(\vec{b} - \vec{b}_A - \vec{b}_B) \times d\vec{b}_A dz_A d\vec{b}_B dz_B, \quad (6.1)$$

where ρ_A (or similarly ρ_B) is the normalized density distribution for the nucleus A (or B) and $t(\vec{b})$ is the normalized thickness function for nucleon-nucleon collision. The spatial coordinates \vec{b}_A, z_A (or similarly \vec{b}_B, z_B) are measured with respect to the center of the nucleus A (or B). The functions ρ , T , and t are normalized as

$$\int \rho_A(\vec{r}) d\vec{r} = \int \rho_B(\vec{r}) d\vec{r} = \int T(\vec{b}) d\vec{b} = \int t(\vec{b}) d\vec{b} = 1. \quad (6.2)$$

The probability for the incident nucleon to make an inelastic collision with a target nucleus is given by the product $T_A(b)\sigma_{in}$, where σ_{in} is the nucleon-nucleon inelastic cross section and is³¹ 31.3 mb. Thus, in any encounter between two nuclei with mass numbers A and B , the probability for the occurrence of n inelastic nucleon-nucleon collisions at an impact parameter b is given by

$$P(n, \vec{b}) = \binom{AB}{n} [T(b)\sigma_{in}]^n [1 - T(b)\sigma_{in}]^{AB-n}, \quad (6.3)$$

which is normalized according to

$$\sum_{n=0}^{AB} P(n, \vec{b}) = 1. \quad (6.4)$$

Note that in the above normalization we include the case of no inelastic collision $n=0$ because the defining event involves any encounter between nucleus A and B .

In this section we shall specialize to the case of nucleon-nucleus collision with $B=1$. From the probability for the occurrence of n inelastic collisions [Eq. (6.3)] and the momentum distribution after n collisions $D^{(n)}(x)$, the differential cross section $d\sigma^{pA}/dx$ for the process $pA \rightarrow bX$ in the collision of a nucleon with a nucleus of mass number A is

$$\frac{d\sigma^{pA}}{dx} = \int d\vec{b} \sum_{n=0}^A \binom{A}{n} D^{(n)}(x) [T(b)\sigma_{in}]^n \times [1 - T(b)\sigma_{in}]^{A-n}. \quad (6.5)$$

In the above equation, the summation runs from $n=0$ to $n=A$. The $n=0$ term represents the cross section for the proton going through or passing the nucleus without an inelastic collision and can be called noninelastic (or no-collision) cross section $d\sigma_{NC}^{pA}/dx$:

$$\frac{d\sigma_{NC}^{pA}}{dx} = \int d\vec{b} [1 - T(b)\sigma_{in}]^A \delta(1-x). \quad (6.6)$$

The rest of the summation in Eq. (6.5) represents the cross section for the proton having suffered at least one inelastic collision and can be called inelastic collision cross section $d\sigma_{IN}^{pA}/dx$

$$\frac{d\sigma_{IN}^{pA}}{dx} = \int d\vec{b} \sum_{n=1}^A \binom{A}{n} D^{(n)}(x) [T(b)\sigma_{in}]^n \times [1 - T(b)\sigma_{in}]^{A-n}. \quad (6.7)$$

With the knowledge of $D^{(n)}(x)$ as given in the preceding section, Eq. (6.5) can be integrated when $T(b)$ is known. For the simple case of $T(b)$ represented by a Gaussian function⁶

$$T(b) = \frac{1}{2\pi\beta^2} \exp\left[-\frac{b^2}{2\beta^2}\right], \quad (6.8)$$

where β is related to the root-mean-square radius of A , we obtain

$$\frac{d\sigma^{pA}}{dx} = 2\pi\beta^2 \sum_{n=0}^A \sum_{i=0}^{A-n} \binom{A}{n} \binom{A-n}{i} D^{(n)}(x) \frac{f^{n+i}}{n+i} (-1)^i, \quad (6.9)$$

where

$$f = \sigma_{in}/2\pi\beta^2. \quad (6.10)$$

For heavy nuclei, the thickness function is closer to the shape of $(R^2 - b^2)^{1/2}$, and can be approximated better by

$$T(b) = (3/2\pi R^3)(R^2 - b^2)^{1/2} \theta(R - b), \quad (6.11)$$

where R is the sum of the radii of nucleus A and B . The differential cross section is then

$$\frac{d\sigma^{pA}}{dx} = 2\pi R^2 \sum_{n=0}^A \sum_{i=0}^{A-n} \binom{A}{n} \binom{A-n}{i} \times D^{(n)}(x) \frac{f^{n+i}}{n+i+2} (-1)^i, \quad (6.12)$$

where

$$f = 3\sigma_{in}/2\pi R^2. \quad (6.13)$$

The above results may perhaps be appropriate in the region of x where the contribution comes mainly from the incident nucleon having suffered more than one or two collisions, because either approximation gives an adequate description of the central density. However, in the region near $x=1$, where the contribution comes mainly from the incident nucleon having suffered one or at most two collisions, the cross section depends very sensitively on the tail of the density distribution. The Gaussian approximation has a large surface thickness and leads to too large a differential cross section $d\sigma/dx$ near $x=1$, while the sharp-cutoff density has no density tail and leads to too small a differential cross section near $x=1$. For these reasons, we shall not use the results of Eqs. (6.8)–(6.13). Instead, we shall obtain $d\sigma/dx$ numerically using Eq. (6.5) and a thickness function obtained numerically from nuclear density. Because of the small size of the nucleon compared to the nucleus, it is reasonable to approximate ρ_B and t by δ functions to obtain

$$T(\vec{b}) = \int \rho_A(\vec{b}, z_A) dz_A. \quad (6.14)$$

We represent the density function by

$$\rho_A(\vec{b}, z_A) = \frac{\rho_0}{1 + \exp\{[(b^2 + z_A^2)^{1/2} - R_A]/a\}}, \quad (6.15)$$

where ρ_0 is chosen to satisfy the normalization condition (6.2), $R_A = r_0 A^{1/3}$ and a is the diffuseness parameter. Numerical results for $d\sigma/dx$ are obtained as a function of x . We can then obtain $x d\sigma/dx$ which is the invariant cross section integrated over the transverse momenta:

$$x \frac{d\sigma}{dx} = \int E \frac{d^3\sigma}{dp^3} d\vec{p}_T. \quad (6.16)$$

Experimentally, the invariant cross sections $E d^3\sigma/dp^3$ for $pA \rightarrow pX$ reactions are measured for a few values of p_T and the integrated cross section $x d\sigma/dx$ is not available except for $pp \rightarrow pX$.^{31,32} To compare with experimental data, we shall assume that in the range of interest, $0.3 < x < 1.0$, these two cross sections are related by a constant

$$E \frac{d^3\sigma}{dp^3} \Big|_{\substack{pA \rightarrow pX \\ p_T=0.3 \text{ GeV}/c}} = x \frac{d\sigma}{dx} \Big|_{pA \rightarrow bX} \times [0.5 (\text{GeV}/c)^{-2}], \quad (6.17)$$

where the numerical factor is chosen to fit proton data. Implicit in the above calibration is the assumption that the p_T dependence and the proton fraction among baryon products is independent of the mass number and the momentum fraction x . This is a reasonable assumption as the transverse momentum distribution in this range of x is only a weak function of x and the mass number,⁴⁰ and the mass dependence of the cross sections $pA \rightarrow pX$ and $pA \rightarrow nX$ are the same.³²

To calculate the cross section $x d\sigma/dx$ for baryon products, we used the parameters $r_0=1.25$ fm and $a=0.5234$ fm. The theoretical results thus obtained give good agreement with the experimental data (Fig. 2). The data for Pb for small values of x may seem higher than the theoretical curve, but the data need confirmation as the shape of the differential cross section for the $p\text{Pb} \rightarrow pX$ reaction at 24 GeV is different.⁴¹ There, the differential cross section at $x=0.167$ is lower than that at $x=0.75$ by about 30%, in closer agreement with the theoretical curve. The present comparison is admittedly crude, but extensive experimental data are still lacking. The important feature of the theoretical results is that, due to multiple collisions, as the mass number increases, the increase in cross section for small values of x is much faster than the increase near $x \sim 1$. The mass dependence of the cross section in different regions of x is thus approximately reproduced. We note from Eq. (3.7) that the average value of x is reduced by a factor of $\frac{1}{2}$ per collision. Thus, the cross section in the range $0.3 < x < 1$ is mainly associated with one or two inelastic nucleon-nucleon collisions during the passage of the nucleon through the nucleus. This explains why the transverse momentum distribution in this range of x is only a weak function of the mass number and that the ratio of the multiplicity near the projectile fragmentation region for pA reactions $R(pA/pp)$ is about 1. It also leads us to understand the importance of the description of the nuclear density near the surface in analyzing the data in this region of x . A sharp cutoff model or a cylindrical nucleus as used in Ref. 25 may lead to misleading results.

In spite of the approximate agreement, one notes that there are systematic deviations of the data of Barton *et al.* from the theoretical curve and from the data of Eichten *et al.* These deviations call for further experimental and theoretical work to check whether there may be a need for corrections to the simple model.

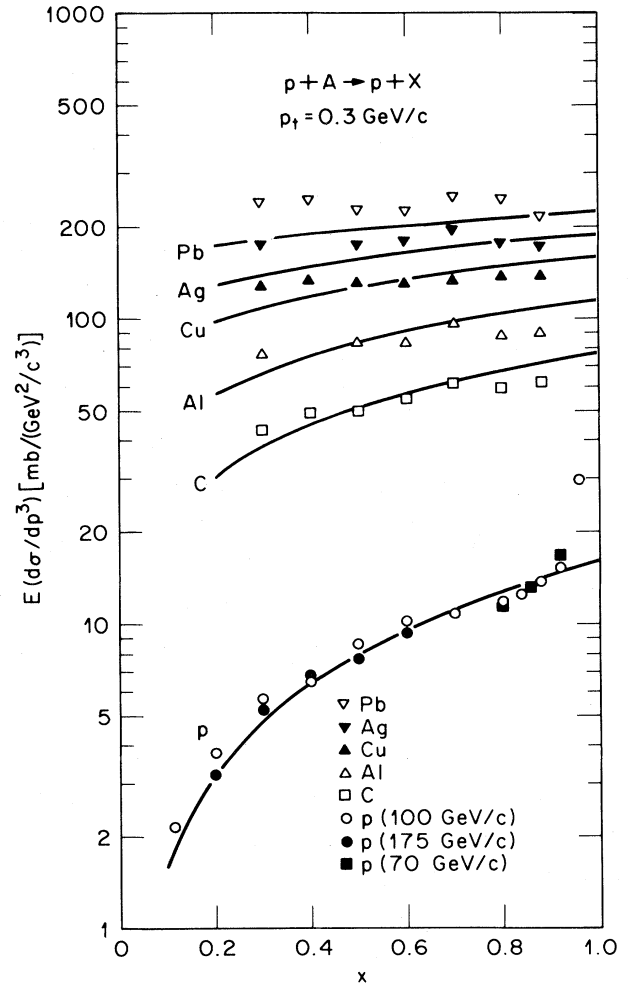


FIG. 2. Comparison of experimental and theoretical (solid curves) invariant cross section for $pA \rightarrow pX$ at 100 GeV/c and $p_t=0.3$ GeV/c.

VII. MOMENTUM DISTRIBUTION IN NUCLEUS-NUCLEUS COLLISIONS

We shall make use of the results of the preceding sections to obtain the momentum distribution for nucleus-nucleus collisions. We can focus our attention on a tube of projectile nucleons arranged in a row impinging on the target nucleus. For the first projectile nucleon, the treatment is just like a nucleon-nucleus collision. For the second projectile nucleon, the nucleon makes collisions with target nucleons many of which have already suffered a collision with the first nucleon and have a momentum distribution with an average rapidity shifted from that of the target rapidity (by about $\Delta y=1.0$ per collision). Feynman scaling gives differential cross sections which do not depend much on the relative energy between the colliding baryons or the energy of the target nucleon. However, the rapidity of the target nucleon enters in the kinematic constraint of the momentum distribution after the collision. Specifically, from Eq. (5.8) the projectile nucleon must have a rapidity greater than the rapidity of

the target nucleon which may be nonzero due to prior collisions. The momentum distribution is thus compressed into a slightly smaller region.

For the collision of nuclei at many tens of GeV per nucleon in the center-of-mass system, the range of rapidity is much in excess of $\Delta y = 1.0$. In the evaluation of the projectile-baryon distribution it is reasonable to neglect the shift of the rapidity of the target nucleons even after they suffer a collision. The projectile nucleons also collide among themselves. The shift of rapidity due to such collisions is small compared with the range of rapidity and can be neglected. With these simplifying assumptions, all the projectile nucleons along the tube are alike and degraded in energy in the same manner. We can treat them as an ensemble of spatially correlated but independent nucleons initially located at their local impact parameter \vec{b}_B and having a momentum distribution $\delta(x-1)$. The projectile-baryon distribution dN^B/dx before collision is

$$\frac{dN^B}{dx}(x) = B \int d\vec{b}_B S_B(\vec{b}_B) \delta(x-1), \quad (7.1)$$

where $S_B(\vec{b}_B)$ is the normalized thickness function for nucleus B ,

$$S_B(\vec{b}_B) = \int \rho(\vec{b}_B, z_B) dz_B. \quad (7.2)$$

With the approximation of a small nucleon size, the function $S_B(\vec{b}_B)$ is equal to the thickness function $T_B(\vec{b}_B)$ for a single target nucleon interacting with the projectile nucleus. In a nucleus-nucleus collision at an overall impact parameter \vec{b} , we can write the projectile-baryon distribution before collision in a physically more transparent way:

$$\begin{aligned} \frac{dN^B}{dx} &= B \int d\vec{b}_B T_B(\vec{b}_B) \delta(x-1) \\ &\times \sum_{n=0}^A \binom{A}{n} [T_A(\vec{b} + \vec{b}_B) \sigma_{in}]^n \\ &\times [1 - T_A(\vec{b} + \vec{b}_B) \sigma_{in}]^{A-n}, \quad (7.3) \end{aligned}$$

where the n th term in the summation represents the probability for a nucleon with impact parameter \vec{b}_B to make n collisions with the target nucleons. The summation over n gives unit probability. From our discussions in previous sections, we know that given an initial momentum distribution $\delta(x-1)$, the momentum distribution, after n inelastic collisions, is $D^{(n)}(x)$ as given by Eq. (5.7). Therefore, by multiplying the n th term in the summation in Eq. (7.3) with $D^{(n)}(x)$ in place of $\delta(x-1)$, we obtain the momentum distribution after the projectile nucleus passes through the target nucleus

$$\begin{aligned} \frac{dN^B}{dx}(x) &= B \int d\vec{b}_B T_B(\vec{b}_B) \\ &\times \sum_{n=0}^A \binom{A}{n} D^{(n)}(x) [T_A(\vec{b} + \vec{b}_B) \sigma_{in}]^n \\ &\times [1 - T_A(\vec{b} + \vec{b}_B) \sigma_{in}]^{A-n}. \quad (7.4) \end{aligned}$$

It is easy to see that the integral of (7.4) with respect to x gives the total projectile baryon number B , as it should. We note in passing that Eq. (7.4) includes the term $n=0$ where $D^{(0)}(x) = \delta(x-1)$, representing those nucleons which pass through the target nucleus without an inelastic collision. In terms of the rapidity variable y , the momentum distribution in y is given similarly by

$$\begin{aligned} \frac{dN^B}{dy}(y) &= B \int d\vec{b}_B T_B(\vec{b}_B) \\ &\times \sum_{n=0}^A \binom{A}{n} D^{(n)}(y) [T_A(\vec{b} + \vec{b}_B) \sigma_{in}]^n \\ &\times [1 - T_A(\vec{b} + \vec{b}_B) \sigma_{in}]^{A-n}. \quad (7.5) \end{aligned}$$

Equation (7.4) or (7.5) gives the baryon distribution for the projectile nucleons. The baryon momentum distribution for the target nucleons can be obtained by reversing the role of projectile and target:

$$\begin{aligned} \frac{dN^A}{dy}(y) &= A \int d\vec{b}_A T_A(\vec{b}_A) \\ &\times \sum_{n=0}^B \binom{B}{n} D^{(n)}(y) [T_B(\vec{b}_A - \vec{b}) \sigma_{in}]^n \\ &\times [1 - T_B(\vec{b}_A - \vec{b}) \sigma_{in}]^{B-n}. \quad (7.6) \end{aligned}$$

All the above baryon distributions can be separated into two parts as

$$\frac{dN^B}{dx} = \frac{dN_{IN}^B}{dx} + \frac{dN_{NC}^B}{dx}, \quad (7.7)$$

or

$$\frac{dN^B}{dy} = \frac{dN_{IN}^B}{dy} + \frac{dN_{NC}^B}{dy}, \quad (7.8)$$

where the subscript NC denotes the term $n=0$ in Eqs. (7.3)–(7.6) for those baryons suffering no inelastic collision, and the subscript IN denotes the rest of the summation for those baryons suffering at least one inelastic collision.

VIII. NUCLEON FERMI MOTION

Nucleons in a nucleus have a momentum distribution characterized by the Fermi momentum of the nucleons. This momentum distribution gives a modification to the results we have obtained in the preceding section. It is of interest to examine quantitatively how they are modified.

In the frame in which the nucleus is at rest, the nucleon momentum distribution is given by⁴²

$$dP = N \exp \left[-\frac{c_T^2}{2\sigma^2} - \frac{c_z^2}{2\sigma^2} \right] \frac{d\vec{c}_T dc_z}{E_0}, \quad (8.1)$$

where $\sigma \sim 100$ MeV/ c . The component c_z can be written in terms of x and c_T :

$$c_z = -\frac{1}{2mx} [m^2(1-x^2) + c_T^2]. \quad (8.2)$$

In order to obtain the momentum distribution in x , it is necessary to integrate over the transverse momentum c_T . In the integration we can neglect terms of order c_T^4/m^2 in comparison with terms of order c_T^2 as the former is of the order of σ^2/m^2 of the latter. We then obtain

$$P(x) = \frac{4N\pi\sigma^2x}{x^2+1} \exp\left[-\frac{m^2(1-x^2)^2}{8x^2\sigma^2}\right]. \quad (8.3)$$

The distribution peaks at $x=1$ with a width of $\sigma_x = \sigma/m = 0.1$; it is reasonable to approximate the above by a normalized distribution centering at $x=1$ with a width σ_x :

$$P(x) = \frac{1}{\sqrt{2\pi}\sigma_x} \exp\left[-\frac{(x-1)^2}{2\sigma_x^2}\right], \quad (8.4)$$

where x can exceed unity. The momentum distribution of projectile baryons in x in a nucleus-nucleus collision is then

$$\frac{dN}{dx}(x) = \int \frac{dN}{dx'}(x')dx' \frac{1}{\sqrt{2\pi}\sigma_x x'} \exp\left[-\frac{(x/x'-1)^2}{2\sigma_x^2}\right] \quad (8.5)$$

and the corresponding distribution in y is given by

$$\begin{aligned} \frac{dN}{dy}(y) &= \int \frac{dN}{dy'}(y')dy' \frac{1}{\sqrt{2\pi}\sigma_x} \\ &\times \exp\left[-\frac{[\exp(y-y')-1]^2}{2\sigma_x^2}\right] \exp(y-y'). \end{aligned} \quad (8.6)$$

It is clear from Eq. (8.5) that nucleon Fermi motion affects mainly the distribution near $x \approx 1$. For the region $x \ll 1$ the effective width is $x\sigma_x$ which becomes very small and the folding distribution is like a δ function. Therefore, the distribution away from $x=1$ is not much affected by the nuclear Fermi motion.

IX. BARYON SPATIAL DENSITY

From the rapidity distribution, we can get the baryon spatial density if all the baryons emerge from the collision at the same time. This corresponds to assuming a zero width for the initial nuclei. It is a good approximation if one is considering those regions of rapidities far from the rapidity of the parent nucleus such as in the central rapidity region. A particle with the rapidity y will be found at the longitudinal coordinate z in the equal-velocity frame, i.e., the projectile-nucleon-target-nucleon center-of-mass frame):

$$z = \tau \sinh(y - y_m), \quad (9.1)$$

where τ is the proper time

$$\tau = (t^2 - z^2)^{1/2}, \quad (9.2)$$

and y_m is the rapidity of the equal-velocity frame

$$y_m = \frac{1}{2} \ln[\exp(y_B) - \exp(-y_B)] \approx y_B/2. \quad (9.3)$$

We have chosen the unit that the speed of light c is equal to unity. The (proper) density at z is defined as the density in the frame in which the particles at z are at rest (longitudinally). Upon averaging over the transverse overlap area \mathcal{A} , the proper density at z due to projectile baryons can be shown to be

$$\rho^{(B)}(z) = \frac{1}{\tau\mathcal{A}} \frac{dN^B}{dy}[y(z)]. \quad (9.4)$$

Both the rapidity distribution dN^B/dy and the overlap area \mathcal{A} depend on the impact parameter. We limit our attention on the case of head-on collision with $b=0$ and at the proper time $\tau=1$ fm/c when the produced particles begin to emerge.¹ The baryon density due to the projectile is

$$\rho^{(B)}(z) = \frac{1}{\pi R_A^2} \frac{dN^B}{dy}[y(z)]/1 \text{ fm}. \quad (9.5)$$

There is a similar density due to the target nucleus:

$$\rho^{(A)}(z) = \frac{1}{\pi R_A^2} \frac{dN^A}{dy}[y(z)]/1 \text{ fm}. \quad (9.6)$$

And, the total baryon density is the sum of these two densities:

$$\rho(z) = \rho^{(A)}(z) + \rho^{(B)}(z). \quad (9.7)$$

X. BARYON DISTRIBUTION IN NUCLEUS-NUCLEUS COLLISIONS

With the formalism presented in the preceding sections, we calculate the baryon momentum distribution dN^B/dy for head-on collisions of two equal nuclei. We shall display the distributions only for the projectile baryons as the target baryon can be obtained by a simple reflection with respect to the central rapidity axis.

The reaction products can be divided into a no-collision (NC) part and an inelastic (IN) part. The former corresponds to those projectile nucleons which pass through the target nucleus without an inelastic collision. They have a sharp momentum distribution centered around the beam rapidity and modified by Fermi motion. Their fraction diminishes as the mass number increases. We list in Table I the number and the fraction of projectile nucleons which do not make an inelastic collision in passing through the target nucleus in a head-on collision.

The momentum distribution of the inelastic projectile baryons in a head-on collision of two equal nuclei is shown in Fig. 3. In Fig. 3(a) the quantity $(dN_{IN}^B/dy)/\pi R_A^2$ is exhibited as a function of $y - y_B$ for a center-of-mass energy per nucleon of $E^* = 30$ GeV per nucleon and for various nuclear masses. At regions far away from the beam rapidity the quantity $(dN_{IN}^B/dy)/\pi R_A^2$ divided by 1 fm gives the proper density at the proper time $\tau=1$ fm/c at which time the produced particles begin to emerge. One finds from Fig. 3 that for light nuclei, the distributions center around the beam rapidity with narrow width. As the mass of the colliding nuclei increases, the peak of the projectile-baryon distribution moves to a lower rapidity. For Pb on Pb, the

TABLE I. Number and fraction of projectile nucleons which suffer no inelastic collision in a head-on collision of two equal nuclei.

Projectile	Target	Number of projectile nucleons which suffer no collision	Fraction of projectile nucleons which suffer no collision
${}^4\text{He}$	${}^4\text{He}$	2.160	0.540
${}^{12}\text{C}$	${}^{12}\text{C}$	4.540	0.378
${}^{16}\text{O}$	${}^{16}\text{O}$	5.351	0.334
${}^{27}\text{Al}$	${}^{27}\text{Al}$	6.979	0.258
${}^{63}\text{Cu}$	${}^{63}\text{Cu}$	9.842	0.156
${}^{108}\text{Ag}$	${}^{108}\text{Ag}$	11.694	0.108
${}^{208}\text{Pb}$	${}^{208}\text{Pb}$	13.946	0.067
${}^{238}\text{U}$	${}^{238}\text{U}$	14.416	0.061

peak shifted to $y - y_R \approx -2.3$, in rough agreement with the average shift of rapidity estimated previously.⁹ However, the width of the projectile-baryon distribution is very wide. It extends well to the target rapidity region of $y - y_B = -8.31$. The increase in the distribution in these regions arises from the large number of nucleon-nucleon inelastic collisions a nucleon suffers in traversing the other nucleus.

In Fig. 3(b) the same quantity $(dN_{\text{IN}}^B/dy)/\pi R_A^2$ is exhibited as a function of $y - y_B$ for a center-of-mass energy $E^* = 100$ GeV per nucleon. By comparing these results with those at $E^* = 30$ GeV per nucleon, one finds that the distributions for ${}^4\text{He} + {}^4\text{He}$ and ${}^{16}\text{O} + {}^{16}\text{O}$ are not changed at all. The distributions for ${}^{63}\text{Cu} + {}^{63}\text{Cu}$ and ${}^{208}\text{Pb} + {}^{208}\text{Pb}$ are hardly changed for rapidity $y - y_B \geq -4$; they are modified mainly in the region $y - y_B \leq -4$. For these medium and heavy nuclei the distributions are stretched more into the lower rapidity region and the accumulation near the target rapidity $y - y_B = -10.72$ is less than the corresponding accumulation at lower energies.

Of particular interest is the baryon spatial density in the central rapidity region (Table II). It has contributions from both the projectile nucleus and the target nucleus. For $E^* = 30$ GeV the baryon density ρ_B in the central rapidity region and $\tau = 1$ fm/c is about 0.04 baryons/fm³ for ${}^{16}\text{O} + {}^{16}\text{O}$, 0.14 baryons/fm³ for ${}^{63}\text{Cu} + {}^{63}\text{Cu}$, and 0.28 baryons/fm³ for ${}^{208}\text{Pb} + {}^{208}\text{Pb}$. For the higher energy $E^* = 100$ GeV per nucleon, the total baryon density in the

central rapidity region and $\tau = 1$ fm/c is about 0.02 baryons/fm³ for ${}^{16}\text{O} + {}^{16}\text{O}$, 0.08 baryons/fm³ for ${}^{63}\text{Cu} + {}^{63}\text{Cu}$, and 0.22 baryons/fm³ for ${}^{208}\text{Pb} + {}^{208}\text{Pb}$.

For comparison, the initial energy density ϵ of hadron matter in the central rapidity region for head-on collisions of two equal nuclei each with a mass number A is⁶

$$\epsilon = 0.06A^{0.70}(0.48 \ln E^* + 0.37) \text{ GeV/fm}^3, \quad (10.1)$$

where E^* , the center-of-mass energy per nucleon, is in GeV. If all the matter become deconfined quark-gluon matter, the net baryon fraction is given by $\rho_B m_T c^2 / (\epsilon + \rho_B m_T c^2)$. This impurity fraction is about 0.05–0.06 for $E^* = 30$ GeV per nucleon and is about 0.02–0.03 for $E^* = 100$ GeV per nucleon (Table II). These are the impurity levels of baryons one has to contend with in the design of accelerators for relativistic heavy-ion collisions.

In other regions of the rapidity variable, one can superimpose the projectile distribution and the target distribution to obtain the total momentum distribution. For light nuclei, the central rapidity region is much lower than the peaks in the projectile rapidity region or in the target rapidity region. However, with the increase in the mass number, the distribution in the central rapidity region has about the same magnitude as does the distribution in the other regions. The composite distribution becomes relatively flat and the baryon impurity is approximately the same over the whole region.

TABLE II. Net baryon-number density ρ_B and quark-gluon-plasma energy density ϵ at the central-rapidity point for two different bombarding energies. The fraction of net baryon energy density $\rho_B m_T c^2 / (\epsilon + \rho_B m_T c^2)$ is given in the last column.

c.m.				
Bombarding energy per nucleon (GeV)	Nuclei	ρ_B (baryons/fm ³)	ϵ (GeV/fm ³)	$\frac{\rho_B m_T c^2}{\epsilon + \rho_B m_T c^2}$
30	${}^{16}\text{O} + {}^{16}\text{O}$	0.0418	0.837	0.049
	${}^{63}\text{Cu} + {}^{63}\text{Cu}$	0.139	2.18	0.061
	${}^{208}\text{Pb} + {}^{208}\text{Pb}$	0.282	5.04	0.054
100	${}^{16}\text{O} + {}^{16}\text{O}$	0.0200	1.08	0.019
	${}^{63}\text{Cu} + {}^{63}\text{Cu}$	0.0855	2.81	0.030
	${}^{208}\text{Pb} + {}^{208}\text{Pb}$	0.217	6.49	0.033

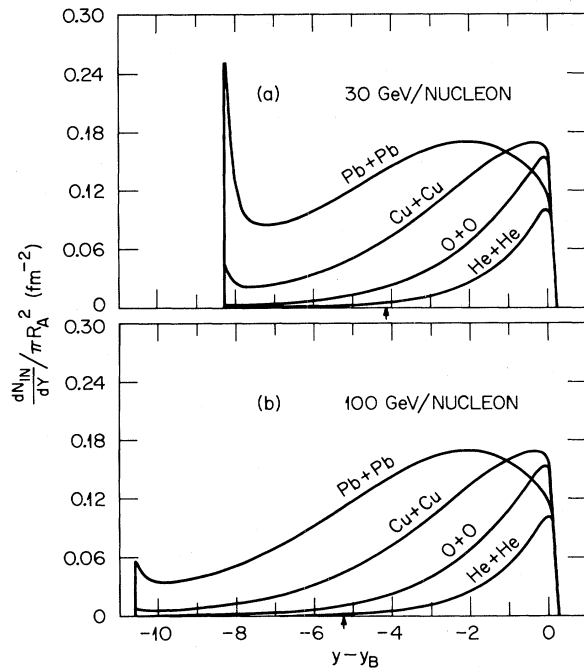


FIG. 3. The projectile-baryon rapidity distribution for head-on collisions of two equal nuclei at two different bombarding energies: (a) at $E^* = 30$ GeV per nucleon and (b) at $E^* = 100$ GeV per nucleon. The central-rapidity point is indicated by an arrow.

XI. SUMMARY AND DISCUSSION

In a nucleon-nucleon collision at high energies, the elastic scattering process has little effect in degrading the energy of the incident nucleon. The degradation arises from inelastic scattering with the production of a large number of particles. Interestingly enough, the resultant baryon has a momentum fraction which is approximately uniformly distributed over the whole range of momentum fractions. On the average, about half of the initial momentum is lost in each inelastic collision.

The basic distribution from an inelastic nucleon-nucleon collision allows us to trace the momentum distribution of nucleons in a nucleon-nucleus collision and a nucleus-nucleus collision. We follow the multiple-collision model of Glauber which was found previously to give a good description of the multiplicity distribution in the central rapidity region.⁶ We made the further as-

sumption that baryon-baryon collisions degrade momenta and produce particles as in free space in order to have a reference model to compare with experiment and to make simple estimates. Results for nucleon-nucleus collisions compare well with the experimental data of Barton *et al.*³² However, there are some differences in the region of small x which need to be further investigated experimentally and theoretically, as experimental data from a different group at a lower energy give a different shape and magnitude.⁴¹

The width of the momentum distribution increases with the number of collisions. The momentum distribution for collisions of heavy nuclei is therefore very broad. It is not enough to know only the average rapidity shift of a reaction as the width can be broader than the shift for heavy nuclei. Furthermore, the kinematic constraint from the energy-conservation condition gives rise to an accumulation of nucleons of one nucleus around the rapidity of the other nucleus when the thickness of the colliding nuclei is great enough to slow down the incident nucleons substantially.

Looking at the baryon distribution results, one finds that except for light nuclei, the total baryon density in the central rapidity region is of the order of the equilibrium nucleon matter density. This total baryon density decreases slightly as the bombarding energy increases. In addition, the number of hadrons produced increases slightly as the bombarding energy increases. Thus, the fractional baryon energy density in the central rapidity region decreases from about 0.06 to about 0.03 as the bombarding energy increases from $E^* = 30$ to 100 GeV per nucleon.

Our result indicates that in the energy range of $E^* \sim 30$ –100 GeV per nucleon, there is a few percent baryon impurity in the central rapidity region due to the broad distribution arising from multiple collisions. A quark-gluon plasma with this amount of baryon impurity can still be of interest and may allow a closer extrapolation to quark-gluon plasma of even smaller baryon fractions for cosmological studies.

ACKNOWLEDGMENTS

The author wishes to thank Professor W. Busza and Professor A. S. Goldhaber for helpful discussions. The research was sponsored by the Division of Nuclear Physics, U. S. Department of Energy under Contract No. DE-AC05-84OR21400 with Martin Marietta Energy Systems, Inc.

¹J. D. Bjorken, Phys. Rev. D **27**, 140 (1983).

²K. Kanjantje and L. McLerran, Phys. Lett. **119B**, 203 (1982).

³T. D. Lee, Columbia University Report No. CU-TP-226, 1981 (unpublished).

⁴M. Gyulassy, Lawrence Berkeley Report No. LBL-15175, 1982 (unpublished).

⁵J. Rafelski and M. Danos, Natl. Bur. Stand. (U.S.) Report No. NBSIR 83-2725, 1983 (unpublished).

⁶C. Y. Wong, Phys. Rev. D **30**, 961 (1984).

⁷For example, L. McLerran and B. Svetitsky, Phys. Lett. **96B**,

195 (1981); Phys. Rev. C **24**, 450 (1981); I. Montvay and H. Pietarinen, Phys. Lett. **115B**, 151 (1982); J. Kogut *et al.*, Phys. Rev. Lett. **48**, 1140 (1982).

⁸D. Schramm, Fermilab Report No. Conf-83/83-AST, 1983 (unpublished); D. Schramm and K. A. Olive, Nucl. Phys. **A418**, 447c (1984).

⁹W. Busza and A. S. Goldhaber, Phys. Lett. **139B**, 235 (1984); W. Busza, Nucl. Phys. **A418**, 635c (1984).

¹⁰J. Kapusta, Phys. Rev. C **27**, 2037 (1983).

¹¹A brief discussion of the present work appeared in C. Y.

- Wong, Phys. Rev. Lett. **52**, 1393 (1984).
- ¹²R. J. Glauber, in *Lectures in Theoretical Physics*, edited by W. E. Brittin and L. G. Dunham (Interscience, New York, 1959), Vol. 1, p. 315.
- ¹³R. Blankenbecler, A. Capella, J. Tran Thanh Van, C. Pajares, and A. V. Ramallo, Phys. Lett. **107B**, 106 (1981).
- ¹⁴V. N. Gribov, Zh. Eksp. Teor. Fiz. **57**, 1306 (1969) [Sov. Phys. JETP **30**, 709 (1970)].
- ¹⁵L. Bertocchi, Nuovo Cimento **11A**, 45 (1972).
- ¹⁶J. H. Weis, Acta Phys. Pol. **B7**, 851 (1976).
- ¹⁷A. Capella and A. Krzywicki, Phys. Lett. **67B**, 84 (1977).
- ¹⁸A. S. Carroll *et al.*, Phys. Lett. **80B**, 319 (1979).
- ¹⁹C. Y. Wong (unpublished).
- ²⁰J. E. Elias, W. Busza, C. Haliwell, D. Luckey, L. Votta, and C. Young, Phys. Rev. Lett. **41**, 285 (1978).
- ²¹J. E. Elias, W. Busza, C. Haliwell, D. Luckey, P. Swartz, L. Votta and C. Young, Phys. Rev. D **22**, 13 (1980).
- ²²W. Busza, in *Proceedings of 4th High Energy Heavy Ion Summer Study, 1978* (Report No. LBL-7766), p. 253.
- ²³A. Capella and A. Krzywicki, Phys. Lett. **67B**, 84 (1977).
- ²⁴K. Kinoshita, A. Minaka, and H. Sumiyoshi, Prog. Theor. Phys. **63**, 928 (1980); **63**, 1268 (1980).
- ²⁵K. Kinoshita, A. Minaka, and H. Sumiyoshi, Prog. Theor. Phys. **61**, 165 (1979); Z. Phys. **8**, 205 (1981).
- ²⁶R. C. Hwa, Phys. Rev. Lett. **52**, 492 (1984).
- ²⁷R. C. Hwa and M. S. Zahir, Report No. OITS-256, 1984 (unpublished).
- ²⁸C. Y. Wong and T. A. Welton, Phys. Lett. **49B**, 243 (1974); H. K. Tang and C. Y. Wong, Phys. Rev. C **21**, 1846 (1980); **26**, 284 (1982).
- ²⁹S. J. Brodsky, Report No. SLAC-PUB-3256, 1983 (unpublished); Report No. SLAC-PUB-3219, 1983 (unpublished); G. T. Bodwin, S. J. Brodsky, and G. P. Lepage, Phys. Rev. Lett. **47**, 1799 (1981); L. Landau and I. Pomeranchuk, Dokl. Akad. Nauk. SSSR **92**, 535 (1953); **92**, 735 (1953); L. Stodolsky, Phys. Rev. Lett. **28**, 60 (1972); A. Bialas and L. Stodolsky, Acta Phys. Pol. **B7**, 845 (1976).
- ³⁰J. D. Bjorken, in *Current Induced Reactions*, (Lecture Notes in Physics No. 56), proceedings of the International Summer School on Theoretical Particle Physics, Hamburg, 1975, edited by J. G. Körner, G. Kramer, and D. Schildknecht (Springer, New York, 1975); J. Kogut and L. Susskind, Phys. Rev. D **10**, 732 (1974).
- ³¹A. E. Brenner *et al.*, Phys. Rev. D **26**, 1497 (1982).
- ³²D. S. Barton *et al.*, Phys. Rev. D **27**, 2580 (1983).
- ³³F. E. Taylor, *et al.*, Phys. Rev. D **14**, 1217 (1976).
- ³⁴O. Benary, L. R. Price, and G. Alexander, Report No. UCRL-20000, 1970.
- ³⁵W. Thome *et al.*, Nucl. Phys. **B129**, 365 (1977).
- ³⁶K. Alpgard *et al.*, Phys. Lett. **107B**, 310 (1981).
- ³⁷E. Fermi, *Nuclear Physics* (University of Chicago Press, Chicago, 1950), p. 182.
- ³⁸R. D. Evans, *The Atomic Nucleus* (McGraw-Hill, New York, 1955).
- ³⁹W. Heitler, *The Quantum Theory of Radiation* (Clarendon, Oxford, 1954).
- ⁴⁰From the limited data available in Ref. 16, the width of the transverse momentum distribution is nearly independent of the target mass number at $x=0.8$. When compared with the proton case, the width increases by about 20% for C and Cu and 10% for Pb at $x=0.5$ and 0.3. The data are too scanty to allow a systematic extraction of the mass dependence and x dependence of the transverse momentum distribution.
- ⁴¹T. Eichten *et al.*, Nucl. Phys. **B44**, 333 (1972).
- ⁴²A. S. Goldhaber, Phys. Lett. **53B**, 306 (1974).